Biased Ostwald ripening in site-selective growth of two-dimensional gold clusters

Rokni Fard, Mahroo; Guo, Quanmin

DOI:
10.1021/acs.jpcc.8b01624

License:
Other (please specify with Rights Statement)

Document Version
Peer reviewed version

Citation for published version (Harvard):
Rokni Fard, M & Guo, Q 2018, 'Biased Ostwald ripening in site-selective growth of two-dimensional gold clusters', *Journal of Physical Chemistry C*, vol. 122, no. 14, pp. 7801-7805.
https://doi.org/10.1021/acs.jpcc.8b01624

Biased Ostwald Ripening in Site-selective Growth of Two-dimensional Gold Clusters

Mahroo Rokni-Fard & Quanmin Guo[*]

School of Physics and Astronomy, University of Birmingham, Birmingham, B15 2TT, United Kingdom

ABSTRACT

Nucleation, growth and ripening of nanoscale Au islands formed on the Au (111) substrate have been investigated using variable temperature scanning tunnelling microscopy (VT-STM). The Au(111) surface consists of two types of naturally occurring dislocations. After deposition of Au atoms at 115 K, a single nano-meter-sized Au island is formed at each dislocation. Thermal annealing to 180 K causes gross mass transport in which Au atoms systematically move from one type of dislocation to the other. This leads to the preferential ripening of Au islands at one of the two types of dislocations, a phenomenon that has not been observed for any other metals deposited in Au(111). With repeated deposition and thermal annealing cycles, we have succeeded in obtaining two types of clusters with very different sizes: large clusters at the bulged elbow site and small clusters at the pinched elbow site.

[*] Corresponding author, Email: Q.Guo@bham.ac.uk

INTRODUCTION

Ostwald ripening is an important process in materials synthesis such as the growth of thin films for perovskite solar cells[1] and supramolecular polymers[2]. As a standard thermodynamic driven process, Ostwald ripening naturally leads to the transfer of material from particles with high chemical potential to particles with low chemical potential[3]. This is commonly observed as the growth of large particles at the expense of the small ones. In some applications such as catalysis, this type of ripening has an undesirable consequence of losing catalytic activities[4]. Recently, there has been a growing interest in controlling Ostwald ripening using kinetic interventions[5,6] with an aim to preventing large particles from growing larger. For example, by patterning a substrate, shape and size control over the formation of a liquid foam can be achieved by altering the size-dependence of the Gibbs free energy[6].

Here we report the growth of Au nanoparticles where Ostwald ripening is modulated by surface patterning. The past few decades have witnessed a rapid growing activity in the synthesis and characterisation of gold nano-materials with a variety of geometries including clusters, rods, plates, shells and cages[7]. One of the promising applications of Au nano-materials is for optical sensing. Consequently, there is a need for accurately placing nanostructured Au on a solid substrate[8]. A popular method for fixing nano-materials to solid surfaces is to choose a patterned substrate as the template. The pattern can be created artificially by lithography for example, or can exist as a natural consequence of surface reconstruction[9]. A well-known surface with a reconstruction-induced pattern is Au (111). Apart from the inertness of gold and the ease in production of large flat terraces, the unique structure of its (111) plane is the main attraction point. Au is the only face centred cubic (FCC) metal with a grossly reconstructed (111) surface. Due to the uniaxial contraction of about 4% in the top layer, surface atoms are periodically moved out of registry from their bulk lattice sites giving rise to alternating FCC and hexagonal close packed (HCP) regions. These two regions are separated by discommensuration lines (DLs) which consist of Au atoms occupying the bridge site. On flat terraces, DLs tend to bend systematically forming the famous herringbone reconstruction pattern[10,11]. The point where a DL bends is known as the elbow site which consists of a surface dislocation. These DLs can be divided into type “x” and “y” based on how they bend at the elbow. An elbow with type-x DL bulging into the FCC

area is known as a bulged elbow, whilst an elbow with rounded type-γ DL pointing to the HCP area is known as a pinched elbow[11-13].

The dislocation network on Au (111) makes this surface a natural template for growing atomic and molecular nanostructures. A large number of investigations have been conducted on the deposition of various metals on Au (111) including Fe[14], Co[15], Ni[12], Mo[16], Pt[17] and Pd[18]. All these metals tend to form islands at the elbow sites after being deposited at room temperature. Depending on the strength of interaction between a particular element and the Au (111) surface, nucleation and growth away from the elbow site can also take place. For instance, when silicon is deposited onto Au (111) at room temperature, Si atoms readily mix with the first layer Au atoms on the flat atomic terraces and the mixing is not influenced by the elbow site[19]. When Ag is deposited on Au (111) in vacuum at RT, Ag atoms are found to form finger-like structures at step edges and the fingers grow non-isotropically into the HCP domain of the reconstructed surface[20]. Using electrochemical deposition, Ag islands are found to form initially inside the HCP domain confined by the DLs [21].

Apart from an early study on the growth of Au on Au (111)[22], there are few publications reporting the behaviour of deposited Au atoms on Au (111). In a recent study, small Au islands formed on Au (111) at the elbow sites after deposition at 110 K have been used to make magic number $(C_{60})_m$ – $(Au)_n$ clusters[23] and nano-rings of molecules[24]. It was also found that the bare Au islands at the elbow sites are not stable beyond 250 K. Although nucleation of metal islands can take place at both the bulged and pinched elbows, the stability of the islands at the two types of elbows is not the same. Here we demonstrate that by thermal activation, Au islands can move from the pinched elbow site to the bulged elbow site, a phenomenon not been reported before. This offers a useful alternative for growing nano-structures on Au (111) by allowing one to preferentially select the bulged elbow site for nucleation and growth. The herringbone reconstruction on Au(111) can be further modified by the width of the atomic terraces[25]. Hence, in principle, one could tailor the surface reconstruction by using vicinal surfaces. Apart from the detailed reconstruction that occurs at the atomic scale, surface morphological changes at larger than micrometer scale can take place on Au(111) under certain experimental conditions[26].

EXPERIMENTAL

Experiments were performed using an Omicron variable temperature scanning tunnelling microscope (VT-STM) inside an ultra-high vacuum chamber with base pressure of 5 x 10^{-10} mbar. Electrochemically etched tungsten tips were used for the STM. Gold samples were prepared by deposition of ~ 300 nm thin film on freshly cleaved highly orientated pyrolytic graphite (HOPG). The Au film was cleaned with at least twelve cycles of Ar^+ ion sputtering and annealing to 1000 K. The sample was then cooled down using liquid nitrogen to reach temperature of 115 K. Once temperature was stabilized Au atoms were deposited using a Createc high temperature effusion cell with deposition rate of 0.005 ML per minute. STM scans were obtained using constant current mode and images were analysed using Image-SXM.

Surface coverage is measured accurately by taking out the tip convolution effect. This is done by comparing the coverage from the STM data and that based on the calibrated flux of the evaporator. The STM raw data tends to over evaluate the amount of Au and this is more a problem for small sized clusters. Using the calibrated flux, we are able to determine the exact amount introduced to the dimensions of the cluster due to tip convolution.

RESULTS AND DISCUSSION

Figure 1a shows an STM image of the Au (111) surface after deposition of 0.041 ML Au atoms at a sample temperature of 115 K. This sample temperature is chosen to make sure that individual Au atoms can reach the surface dislocations via diffusion, and at the same time thermal energy is not high enough to displace an atom already trapped by a dislocation. We find that surface dislocations are unable to retain Au atoms at temperatures above 240 K. The Au islands as shown in Fig. 1a do not appear to have a regular shape. This is probably due to the rather small size of the islands allowing rapid edge diffusion of Au atoms. Increasing the temperature of the sample can help to form more uniform polygonal structures. The Au islands observed on the surface are single atomic layer high as shown in Fig. 1b. Figure 1c shows a schematic diagram illustrating the locations of the Au islands at the two types of elbows. When atoms/molecules are deposited onto Au (111), they land onto either the FCC or the HCP region. In the subsequent diffusion process, if the barrier presented by the DLs is high in comparison with thermal energy, the atom/molecule will be confined by the DLs. If thermal energy is high, an atom/molecule inside the HCP region can

climb over a DL and settle in the adjacent FCC region[27]. In the extreme case, the HCP region keeps on loosing atoms/molecules and all material gather at the bulged elbow site[28]. The preferential segregation of atoms/molecules from the HCP to the FCC region is due to the deeper potential well in the FCC region[28].

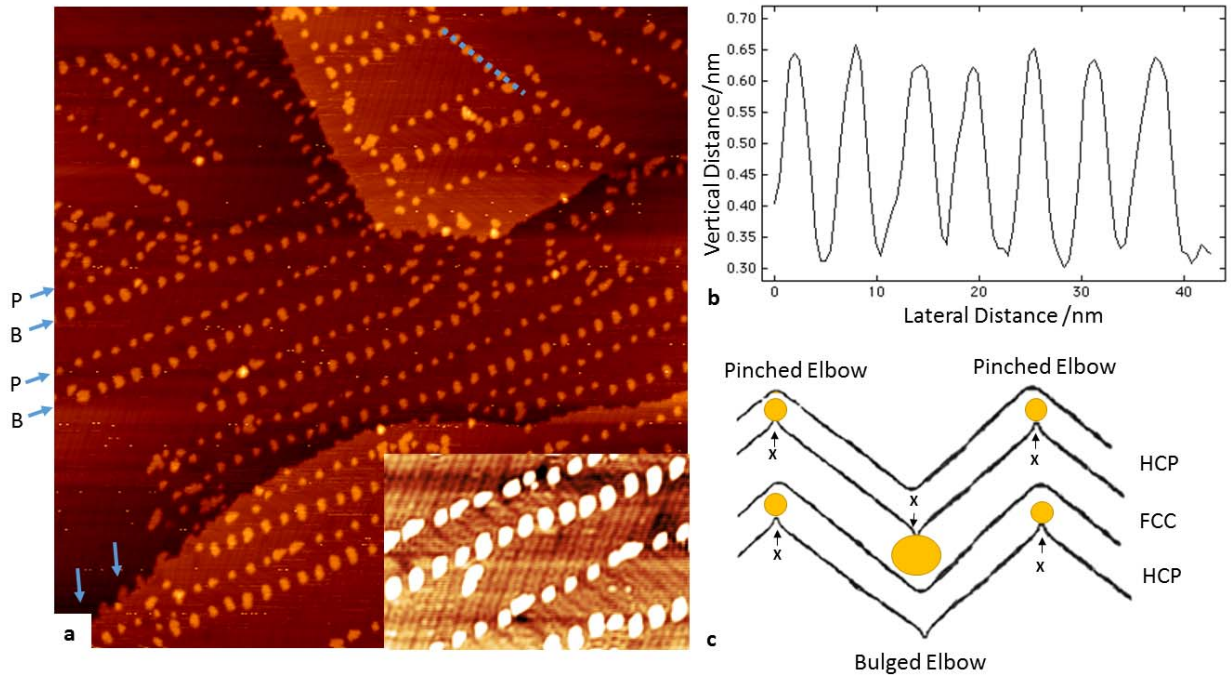

Figure 1: Regular array of two-dimensioanl Au nanoclusters on Au(111). a) STM imaged obtained after deposition of 0.041 ML Au at 115 K. At this coverage Au islands are observed both on pinched elbow (marked as "P"), bulged elbow (marked as "B") and step edges. Inset highlights the surface reconstruction pattern. Height profile of the Au clusters along the dotted blue line shown in (b) confirms that the clusters are single atomic layer high. (c) Schematic diagram showing the two different types of elbows and the positions of the Au islands.

Size distributions for Au islands at different locations: i) bulged elbow, ii) pinched elbow, iii) step edge are shown in Fig. 2. As shown in this figure, size distribution at the bulged elbow is broader than that at the pinched elbow. This is likely due to the larger FCC area available at the bulged elbow allowing the formation of larger clusters. The average size for islands at the bulged elbow and the pinched elbow is 8.1 $nm^2 \pm 3.5$ nm^2, and 4.5 $nm^2 \pm 1.0$ nm^2 respectively. The total amount of Au collected by the bulged elbow site is about 1.8 times of that collected by the pinched elbow site. This indicates little diffusion of Au atoms across the DLs at 115 K with Au atoms landed into the fcc region all captured by the bulged elbows and those landed into the hcp region all captured by the pinched elbows. Small number of Au islands with an average size of 6.5 $\pm$ 4 nm^2 attached to step edges are also observed.

There is no preferential attachment of atoms to steps which compete with the elbow sites for Au atoms.

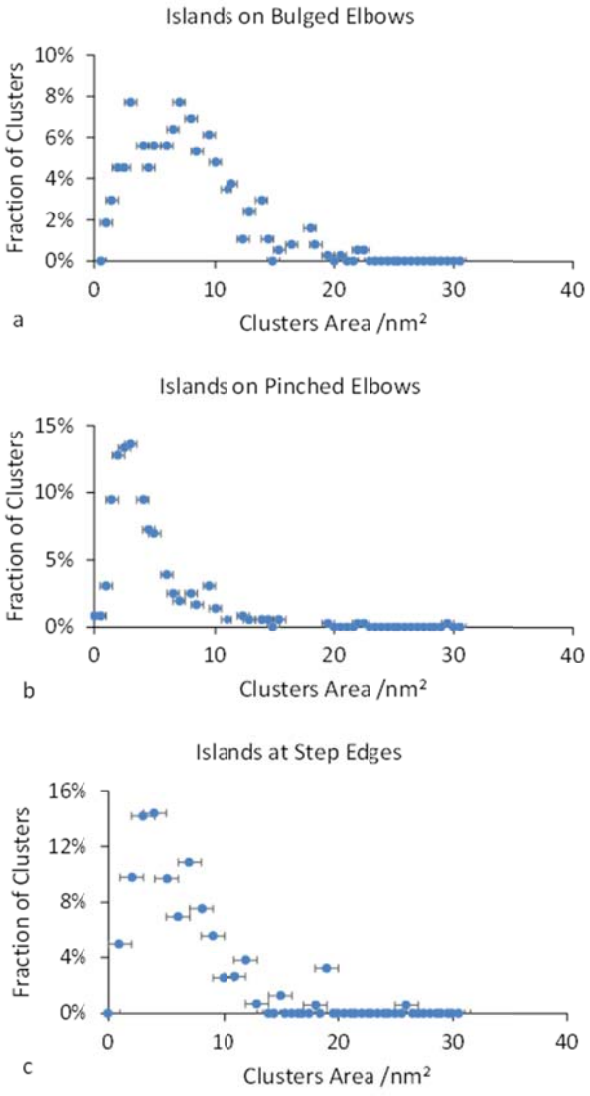

Figure 2: Size distribution of Au clusters on bulged elbow (a), pinched elbow (b) and at step edges (c).

To monitor the ripening process, we increased the sample temperature gradually to 180 K. This temperature is below 240 K and yet is high enough to promote atomic transfer from islands in the HCP region to islands in the FCC region. We followed the structural changes on a Au (111) sample with 0.005 ML of pre-deposited Au. This is much smaller a coverage than that used to make the sample shown in Fig. 1. The smaller starting coverage is advantageous because changes are more significant with smaller sized clusters and hence can be observed within a shorter annealing time. Figure 3a shows an STM image of the sample after being annealed at 180 K for 2 hours. In this figure, the Au islands are found

almost exclusively at the bulged elbows. The majority of pinched elbows, inside the rectangular boxes, have no Au islands attached. In fact, the very small number of Au islands observed close to pinched elbows, Fig. 3a, are not the original islands there. The original islands at the pinched elbows are located inside the HCP region, Fig. 1c. In Fig. 3a, the Au islands near the pinched elbows are found inside the FCC region. Therefore, heating to 180 K has resulted in displacing all Au atoms from the original binding site at the pinched elbows. Most of the displaced Au atoms join existing clusters at the bugled elbows causing the clusters at bulged elbows to grow. A small fraction of atoms form new clusters in the FCC region next to the pinched elbows. Fig. 3b shows the size distribution for the clusters at the bulged elbows before and after thermal annealing. From the data, we find that on average the size of clusters at bulged elbows has increased from ~ 2.5 ± 0.5 nm^2 to ~ 3.0 ± 0.5 nm^2.

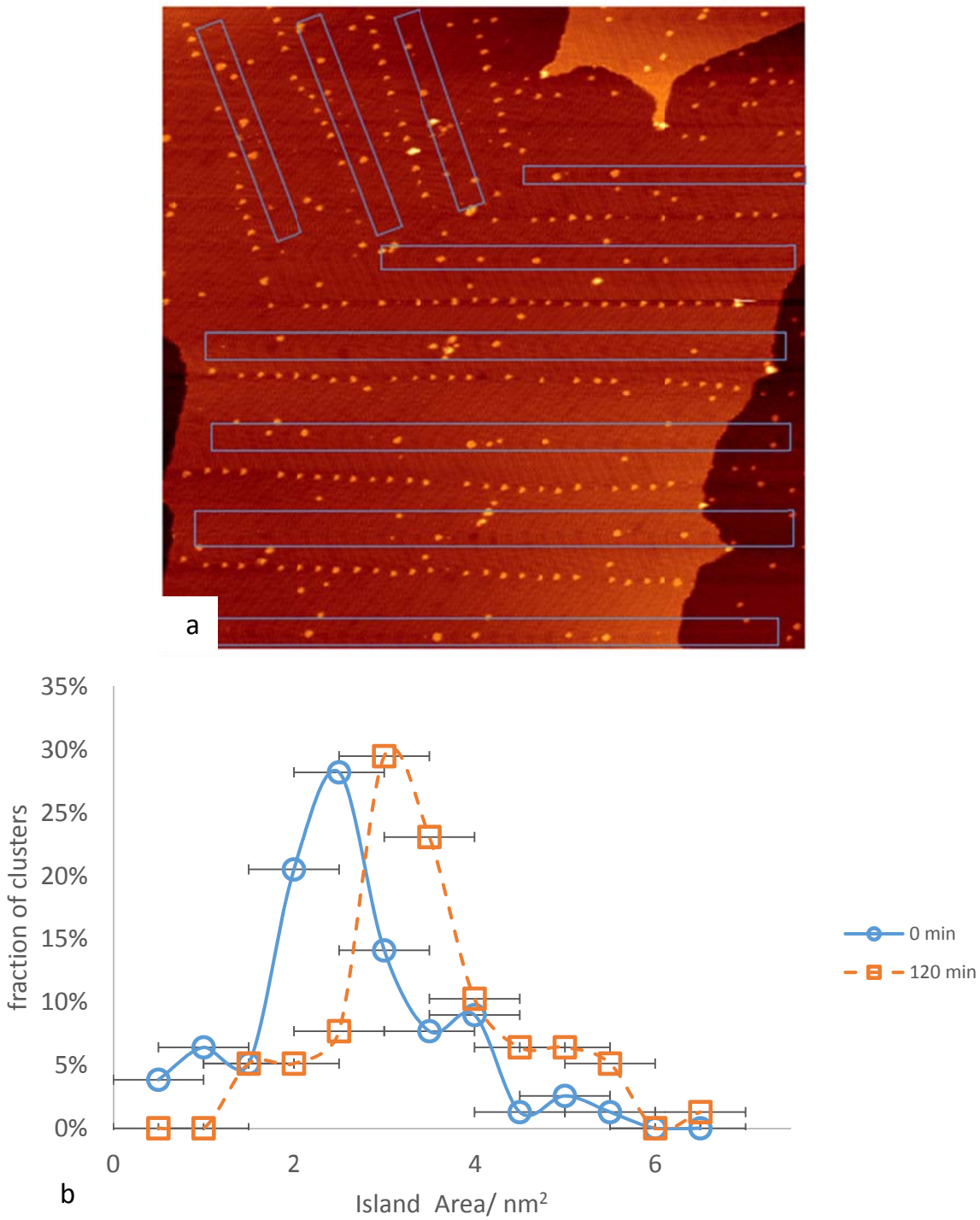

Figure 3: Selective ripening of Au clusters. a) Au islands on the pinched elbows have been removed after annealing the sample for 2 hours at 180 K. Empty pinched elbows are highlighted by blue boxes. Image size is 250.5 nm x 250.5 nm acquired using V= -1.6V and I= 0.05nA. b) Size distribution of Au islands on bulged elbows before (blue) and after (orange) annealing for 2 hours at 180 K.

Fig. 4 shows how the average size of the Au islands changes as a function of annealing time at 180 K. The net effect of annealing at 180 K is hence ripening of the islands at the bulged

elbows and diminishing of islands from the pinched elbows. The total coverage before and after annealing remained constant as mass transport from clusters to step edges is insignificant.

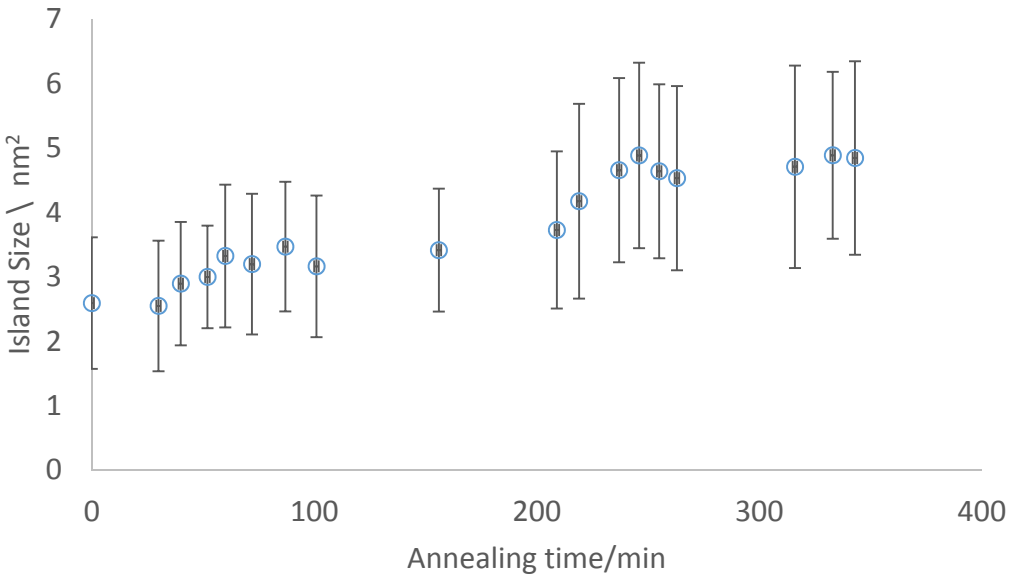

Figure 4: Cluster size as a function of annealing time. The plot is for clusters at the bulged elbow site.

Our findings are consistent with previous studies[28] that the potential well in the FCC region is deeper than that in the HCP region. During annealing, atoms are "evaporated" off the Au islands. Because of the lower potential barrier for Au atoms to jump from the HCP to the FCC region than that of the reverse process, there is a net flow of Au atoms from the HCP region to the FCC region. The extra atoms arriving in the FCC region are incorporated into the existing islands at the bulged elbows. Provided that the annealing time is long enough, complete transfer of Au atoms from the pinched elbows to the bulged elbows can be achieved. Based on the graph of Fig. 4, the island area gradually increases during the first 250 minutes' annealing. After that, the average size remains rather constant. At this point there is no island on HCP areas near pinched elbows. The lack of data points between 130 min and 230 min is due to the limited number of good scans obtained during the experiment.

Thermally induced transfer of atoms from pinched elbows from bulged elbows is a unique property of Au islands on the Au (111) surface. When other metals are deposited onto Au(111), two-dimensional clusters form in a similar way. However, increasing the sample temperature usually leads to inter-mixing of the deposited atoms with the Au atoms in the substrate. On Au(111), the Ostwald ripening process is heavily biased towards the clusters at the bulged elbow site leading to self-selective ripening. This biased ripening phenomenon can be further exploited to control the cluster distribution. We achieved this by performing many deposition-annealing cycles. The procedure is as follows. Small amount of Au is deposited onto Au(111) at 115 K. Thermal annealing at 180 K resulted in emptying all the pinched elbows and growth of clusters at the bulged elbows. The sample is then cooled down to 115 K and more Au is deposited. This is then followed by annealing again at 180 K. By repeating the above processes, we can crate a sample with bimodal cluster distribution with controlled cluster size. Moreover, the small and large clusters occupy distinctly different sites on the surface. Figure 5 is an example of a Au(111) surface after 2 cycles of depositing 0.005 ML Au at 115 K and annealing at 180 K, followed by a final deposition step of 0.005 ML at 115 K. Figure 5B is a magnified view of the area marked by doted rectangle in Fig. 5a. In Fig. 5, the large clusters at the bulged elbows have collected an equivalent of ~0.013 ML of Au and the small clusters are formed mainly by capturing ~ 0.02 ML of Au from the very last deposition. It is possible to repeat these cycles to enlarge the size of Au islands on bulged elbow even more.

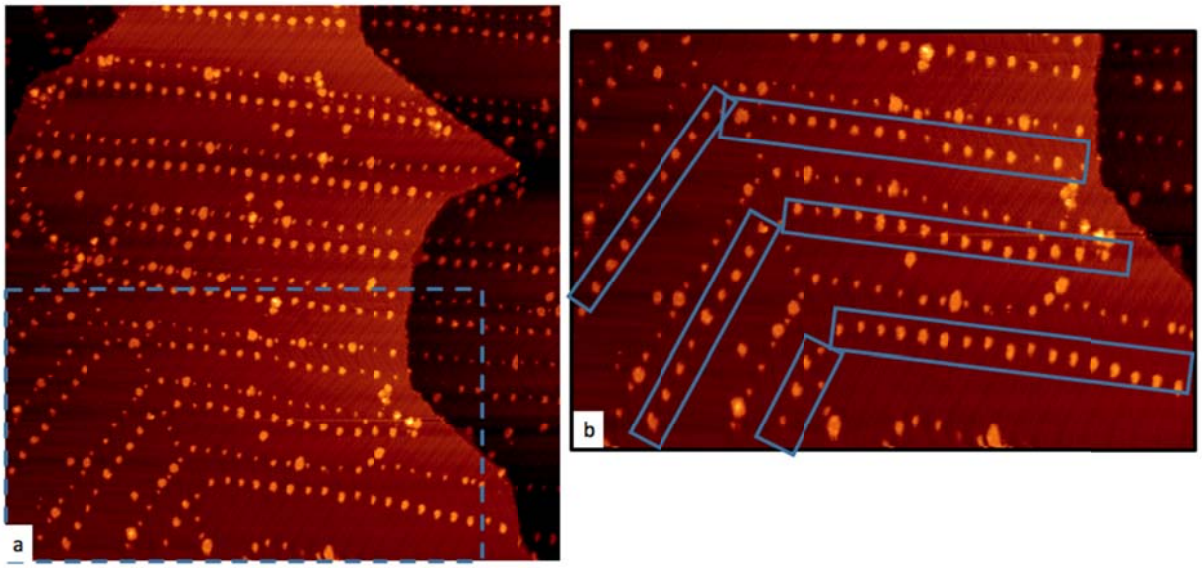

Figure 5: Controlled cluster formation with bimodal distribution via biased Ostwald ripening. a) Surface after 2 cycles of deposition (0.005 ML Au) and annealing at 180 K for 2 hours, followed by a final deposition of another 0.005 ML of Au atoms at 115 K. The total coverage is 0.015 ML. Image size: 253.49 nm x 253.49 nm, obtained with a sample bias of V= -1.93 V, and tunnel current of I= 0.05 nA. b) Zoomed in image of the area marked in (a). In this image larger islands on bulged elbows are highlighted by blue rectangles.

Biased Ostwald ripening is a useful process to grow self-organised nanostructures on surfaces. Previously the formation of $(C_{60})_m$-$(Au)_n$ magic number clusters from deposition of Au and C_{60} molecules has been reported[23,29]. The magic number clusters are formed at both the bulged and the pinched elbows. Using biased Ostwald ripening, we have now successfully produced magic number $(C_{60})_m$-$(Au)_n$ clusters preferentially located on the bulged elbows. As can be seen in Figure 6, more than 80 % of $(C_{60})_m$-$(Au)_n$ magic clusters are formed on the bulged elbow. Biased Ostwald ripening is a rather general phenomenon that deserves some more detailed investigation. Adibi *et al* have reported an interesting ripening process of Pt nano particles on an artificially patterned alumina substrate[30]. The contribution of heterogeneity on the substrate towards biased Ostwald ripening has been studied using Monte Carlo simulations[31,32]. The simulations led to a rather good consistency with our experimental findings.

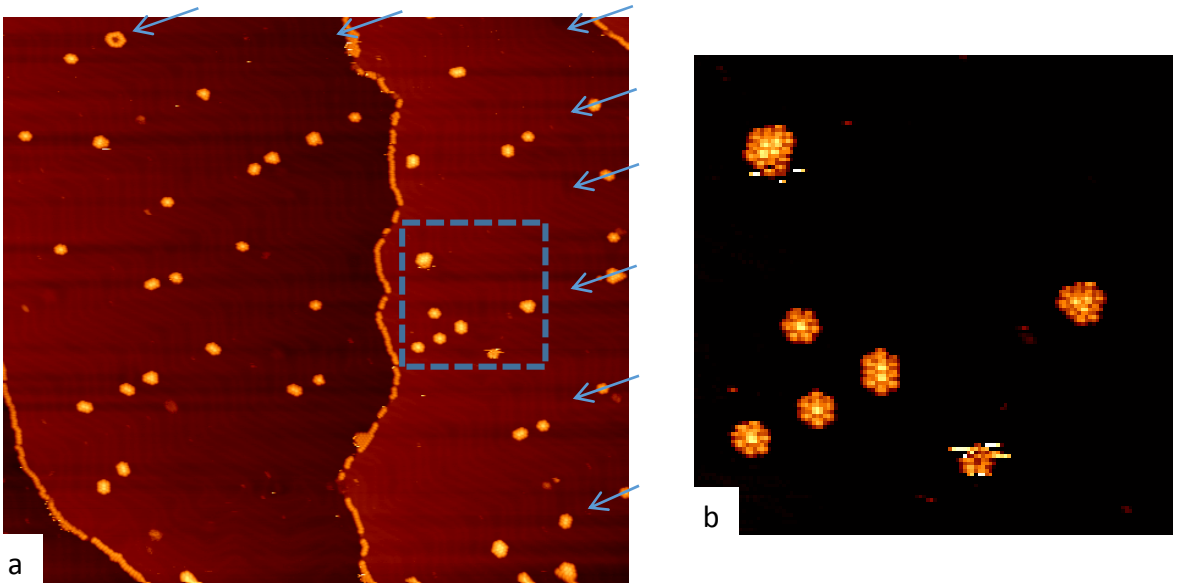

Figure 6: Rows of magic number $(C_{60})_m$-$(Au)_n$ clusters pinned at bulged elbows marked by blue arrows. Pinched elbows are not occupied by clusters. (a) Image size: 189.37 nm x 189.37 nm, Sample bias is V = –2.14 V and tunnel current is I = 0.05 nA. (b) A magnified view of the area inside the square box in (a). There are three clusters with 7 C_{60} molecules, one with 10 C_{60} molecules and one 12 C_{60} molecules.

In summary we have successfully demonstrated biased Ostwald ripening on Au(111). Au clusters can form at both the bulged and the pinched elbow sites at 115 K, but the distinct difference in chemical potential for clusters at the two types of defect sites leads to the preference ripening of clusters at the bulged elbows. This biased ripening proceeds to such an extreme that preformed clusters at the pinched elbow site can be completely removed. The removed material is transferred to clusters at the bulged elbow site with ~ 100% conversion. Cycling the deposition-annealing process allows us to create bimodal cluster distribution with very sharp distribution peaks. The size of the small and the large clusters can be accurately controlled.

REFRERENCES

(1) Yang, M. J.; Zhang, T. Y.; Schulz, P.; Li, Z.; Li, G.; Kim, D. H.; Guo, N. J.; Berry, J. J.; Zhu, K.; Zhao, Y. X. Facile fabrication of large-grain $CH_3NH_3PbI_{3-x}Br_x$ films for high-efficiency solar cells via CH_3NH_3Br-selective Ostwald ripening. *Nat. Commun*. **2016**, *7*, 12305.

(2) Levin, A.; Mason, T. O.; Adler-Abramovich, L.; Buell, A. K.; Meisl, G.; Galvagnion, C.; Bram, Y.; Stratford, S. A.; Dobson, C. M.; Knowles, T. P. J. *et al*, Ostwald's rule of stages governs structural transitions and morphology of dipeptide supramolecular polymers, *Nat. Commun*. **2014**, *5*, 5219.

(3) Lifshitz, I.; Slyozov, V. The kinetics of precipitation from supersaturated solid solutions. *J. Phys. Chem. Solids* **1961**, *19*, 35-50.

(4) Wettergren, K.; Schweinberger, F. F.; Deiana, D.; Ridge, C. J.; Crampton, A. S.; Rotzer, M. D.; Hansen, T. W.; Zhdanov, V. P.; Heiz, U.; Langhammer, C. High sintering resistance of size-selected platinum cluster catalysts by supressed Ostwald ripening. *Nano Lett*. **2014**, *14*, 5803-5809.

(5) Xin, H. L.; Zheng, H. In situ observation of oscillatory growth of bismuth nanoparticles. *Nano Lett*. **2012**, *12*, 1470-1474.

(6) Huang, Z. D.; Su, M.; Yang, Q.; Li, Z.; Chen, S. R.; Li, Y. F.; Zhou, X.; Li, F. Y.; Song, Y. L. A general patterning approach by manipulating the evolution of two-dimensional liquid foams. *Nat. Commun*. **2017**, *7*, 14110.

(7) Yang, X.; Yang, M.; Pang, B.; Vara, M.; Xia, Y. Gold nanomaterials at work in biomedicine. *Chem. Rev*, 2**015**, *115*, 10410-10488.

(8) Neretina, S.; Hughes, R. A.; Gilroy, K. D.; Hajfathalian, M. Noble metal nanostructure synthesis at the liquid–substrate interface: New structures, new insights, and new possibilities. *Acc. Chem. Res*. **2016**, *49*, 2243-2250.

(9) Yu, W.; Porosoff, M. D.; Chen, J. G. Review of Pt-based bimetallic catalysis: from model surfaces to supported catalysts. *Chem. Rev.* **2012**, *112*, 5780-5817.

(10) Van Hove, M. A.; Koestner, R. J.; Stair, P.; Biberian, J. P.; Kesmodel, L. L.; Bartoš, I.; Somorjai, G. A. The surface reconstructions of the (100) crystal faces of iridium, platinum and gold: I. Experimental observations and possible structural models. *Surf. Sci.* **1981**, *103*, 189-217.

(11) Barth, J. V.; Brune, H.; Ertl, G.; Behm, R. J. Scanning tunneling microscopy observations on the reconstructed Au (111) surface: Atomic structure, long-range superstructure, rotational domains, and surface defects. *Phys. Rev. B* **1990**, *42*, 9307-9318.

(12) Chambliss, D. D.; Wilson, R. J.; Chiang, S. Nucleation of ordered Ni island arrays on Au (111) by surface-lattice dislocations. *Phys. Rev. Lett.* **1991**, *66*, 1721-1724.

(13) Besenbacher, F.; Lauritsen, J. V.; Linderoth, T. R.; Lægsgaard, E.; Vang, R. T.; Wendt, S. Atomic-scale surface science phenomena studied by scanning tunneling microscopy. *Surf. Sci*. **2009**, *603*, 1315-1327.

(14) Voigtländer, B.; Meyer, G.; Amer, N. M. Epitaxial growth of Fe on Au (111): a scanning tunneling microscopy investigation. *Surf. Sci.* **1991**, ***255***, L529-L535.

(15) Voigtländer, B.; Meyer, G.; Amer, N. M. Epitaxial growth of thin magnetic cobalt films on Au (111) studied by scanning tunneling microscopy. *Phys. Rev. B* **1991**, *44*, 10354-10357.

(16) Biener, M. M.; Biener, J.; Schalek, R.; Friend, C. M. Surface alloying of immiscible metals: Mo on Au (111) studied by STM. *Surf. Sci.* **2005**, *594*, 221-230.

(17) Pedersen, M. Ø.; Helveg, S.; Ruban, A.; Stensgaard, I.; Lægsgaard, E.; Nørskov, J. K.; Besenbacher, F. How a gold substrate can increase the reactivity of a Pt overlayer. *Surf. Sci.* **1999**, *426*, 395-409.

(18) Casari, C. S.; Foglio, S.; Siviero, F.; Bassi, A. L.; Passoni, M.; Bottani, C. E. Direct observation of the basic mechanisms of Pd island nucleation on Au (111). *Phys. Rev. B* **2009**, *79*, 195402.

(19) Tang, L.; Li, F.; Guo, Q., A structured two-dimensional Au–Si alloy. *Appl. Surf. Sci.* **2011**, *258*, 1109-1114.

(20) Dovek, M. M.; Lang, C. A.; Nogami, J.; Quate, C. F. Epitaxial growth of Ag on Au (111) studied by scanning tunneling microscopy. *Phys. Rev. B* **1989**, *40*, 11973-11975.

(21) Takakusagi, S.; Kitamura, K.; Uosaki, K. In situ real-time monitoring of electrochemical Ag deposition on a reconstructed Au (111) surface studied by scanning tunneling microscopy. *J. Phys. Chem. C* **2008**, *112*, 3073-3077.

(22) Lang, C. A.; Dovek, M. M.; Nogami, J.; Quate, C. F. Au (111) autoepitaxy studied by scanning tunneling microscopy. *Surf. Sci.* **1989**, *224*, L947-L955.

(23) Xie, Y. C.; Tang, L.; Guo, Q. Cooperative Assembly of Magic Number C_{60}-Au Complexes. *Phys. Rev. Lett.* **2013**, *111*, 186101.

(24) Xie, Y. C.; Rokni Fard, M.; Kaya, D.; Bao, D.; Palmer, R. E.; Du, S.; Guo, Q. Site-Specific Assembly of Fullerene Nanorings Guided by Two-Dimensional Gold Clusters. *J. Phys. Chem. C* **2016**, *120*, 10975-10981.

(25) Chauraud, D.; Durinck, J.; Drouet, M.; Vernisse, L.; Bonneville, J.; Coupeau, C. Influence of terrace widths on Au(111) reconstruction. *Phys. Rev. B* **2017**, *96*, 045410.

(26) Lauer, M. E.; Jungmann, R.; Kindt, J. H.; Magonov, S.; Fuhrhop, J-H.; Oroudjev, E.; Hansma, H. Formation of healing of micrometer-sized channel networks on highly mobile Au(111) surfaces. Langmuir, **2007**, *23*, 5459-5465.

(27) Möller, F. A.; Magnussen, O. M.; Behm, R. J. Overpotential-controlled nucleation of Ni island arrays on reconstructed Au (111) electrode surfaces. *Phys. Rev. Lett*. **1996**, *77*, 5249.

(28) Böhringer, M.; Morgenstern, K.; Schneider, W. D.; Berndt, R.; Mauri, F.; De Vita, A.; Car, R. Two-dimensional self-assembly of supramolecular clusters and chains. *Phys. Rev. Lett*. **1999**, *83*, 324.

(29) Kaya, D.; Bao, D.; Palmer, R. E.; Du, S.; Guo, Q. Tip-triggered thermal cascade manipulation of magic number gold-fullerene clusters in the scanning tunneling microscope. *Nano Lett.* **2017**, *17*, 6171-6176.

(30) Adibi, P. T. Z.; Pingel, T,; Olsson, E.; Gronbeck, H.; Langhammer, C. Pt nanoparticle sintering and redispersion on a heterogeneous nanostructured support. *J. Phys. Chem. C* **2016**, *120*, 14918-14925.

(31) Zhdanov, V. P.; Larsson, E. M.; Langhammer, C. Novel aspects of Ostwald ripening of supported metal nanoparticles. *Chem. Phys. Lett*. **2012**, *533*, 65-69.

(32) Zhdanov, V. P. Two-dimensional Ostwald ripening on a patterned support and in a mixed overlayer. *Surf. Sci*. **2016**, *644*, 191-198.

TOC Graphic